SAND88-0616
Unlimited Release
Printed June 1997

Distribution
Category UC-71

Numerical and Analytical Methods for Approximating the Eccentric Impact Response (Slapdown) of Deformable Bodies

G. D. Sjaardema and G. W. Wellman
Applied Mechanics Division I
Sandia National Laboratories
Albuquerque, New Mexico 87185

Abstract

Analytical and numerical methods have been developed to approximate the eccentric impact response of deformable bodies. The eccentric impact response is commonly known as *slapdown* since the off-center impact gives the body a rotational velocity which causes impact at the opposite end. A code, SLAPDOWN, has been written to approximate the slapdown behavior of deformable bodies. The body is idealized as a three degree-of-freedom system with nonlinear impact behavior.

Several parameters of interest to the analysis and design of laydown weapons were studied to determine their effects on the secondary impact velocities (slapdown). Parameters studied are aspect ratio of the body, stiffness of the initial impact, and friction between the target and the body. Rules for applying the results of scale model tests to full scale bodies are developed and confirmed for nonlinear spring behavior.

Contents

Figures

Tables

1. Introduction

There are many cases where the description of rigid body motion during an impact event is desired. Two examples are the response of a radioactive materials transportation container to the regulatory 30-foot drop event and the effects of certain deployment options on various weapon components. Rigid body motion effects are of primary importance for eccentric impact orientations in which a vector normal to the impact surface at the point of impact does not pass through the center of gravity of the body. In this impact orientation, the body will tend to rotate about the impact point which will possibly result in a secondary impact at the opposite end of the body. This sequence of a primary impact followed by a secondary impact at the opposite end of the body is commonly called *slapdown*. In many cases, the secondary slapdown impact can occur at a higher velocity and be more damaging than the primary impact. A computer program called SLAPDOWN has been written to approximate the slapdown behavior of deformable bodies and to aid in the investigation of eccentric impact events.

In this report, the basic analytical approach to the problem of shallow angle slapdown is shown in Chapter 2. The numerical implementation of the solution of the nonlinear equations of motion is developed in Chapter 3. Applications to a variety of generic slapdown issues are presented in Chapters 4–6. These generic issues include the effects of geometric variables, initial impact behavior, and friction on the slapdown severity. Chapter 7 details the proper procedures to follow for extrapolation of scale model test results to the full-scale response. A user's manual detailing the input required and the output from SLAPDOWN is presented in Appendix A. The analytical results from SLAPDOWN are compared to the experimental results from a test program on a half-scale model of an actual radioactive materials transportation container in Appendix B, and Appendix C is a description of the EXODUS database format.

The primary motivation for the development of this capability was to address the behavior of radioactive materials transportation containers during shallow angle slapdown impact events. Therefore, the applications presented reflect container geometries and impact limiter behavior typical of this field. This should not in any way be considered the exclusive use of the computer program.

2. Analytical Prediction of Slapdown Magnitude

2.1 Introduction

In this chapter, simple equations are developed that can economically be used to estimate the ratio of the initial vertical velocity to the secondary impact velocity during a slapdown impact orientation. The equations can also be used to determine the critical impact angle θ_0 producing the largest secondary impact velocity. The only variables required are geometric and mass quantities; the force-displacement behavior of the impact is not required.

2.2 Derivation of Slapdown Equation

The body is approximated by the three degree-of-freedom system shown in Figure 3.1 on page 21. The force-displacement behavior is approximated by springs located at the initial and secondary impact points. The slapdown equation is developed assuming that (1) the springs are linear elastic, (2) there are no horizontal forces due to friction between the rigid surface and the body, and (3) at most one spring is in contact with the rigid surface at any time. Assumption (2) reduces the body to a two degree-of-freedom system, and assumption (3) further reduces it to a sequence of one degree-of-freedom systems. It will be shown that the linear elastic behavior is a conservative assumption that maximizes the secondary impact velocity.

In the text that follows, the nose and tail of the body refer to the initial and secondary impact points, respectively. The sign convention used is that displacements, velocities and accelerations are positive downward; and angular positions, velocities and accelerations are positive clockwise.

2.2.1 Nomenclature

The nomenclature used in the derivation of the Slapdown equation is defined below.

y,$\dot{y}$,$\ddot{y}$ Vertical displacement, velocity, and acceleration. Positive toward rigid surface,

θ,ω,α Angular inclination, velocity, and acceleration of the axis of the body with respect to the rigid surface, positive counterclockwise if the nose is to the left of the tail,

m,I_{CG} Body mass and moment of inertia about the center of gravity,

l Length from the center of gravity to the impact point measured along the axis of the body,

k Spring constant (force/length),

v_0,θ_0 Initial vertical velocity and angular position of the body,

ω_n Natural frequency of the differential equation, and

t Time.

For the geometric variables and the linear displacement quantities, the subscripts $(\cdot)_n$ and $(\cdot)_t$ designate the nose and tail of the body, respectively; a superposed dot indicates the time derivative of the dotted quantity.

2.2.2 Rigid Body Motion Equations

Using D'Alembert's principle, the vertical acceleration $\ddot{y}_n$ at the nose and the angular acceleration α about the nose during the time interval that only the nose is in contact with the rigid surface can be determined by the summation of moments and forces.

$$\sum M_n \to 0 = 2\ddot{y}_n l_n + \alpha(l_n - r)^2 + \alpha(l_n + r)^2 \tag{2.1}$$

$$\sum F_n \to -ky_n = \frac{m}{2}\{[(l_n - r)\alpha + \ddot{y}_n] + [(l_n + r)\alpha + \ddot{y}_n]\} \tag{2.2}$$

where: r is the radius of gyration $= \sqrt{\frac{I_{CG}}{m}}$,
l_n is the distance from the center of mass to the nose,
y_n is the vertical displacement of the nose,
k is the elastic spring constant, and
it is assumed that $\cos\theta \approx 1$.

Equation (2.1) can be used to give α in terms of $\ddot{y}_n$:

$$\alpha = \frac{-\ddot{y}_n l_n}{l_n^2 + r^2} \tag{2.3}$$

Using this result, Equation (2.2) can be written as the single degree-of-freedom equation:

$$\ddot{y}_n \left[\frac{m}{\beta_n^2 + 1}\right] + ky_n = 0 \tag{2.4}$$

where β_n is defined to be l_n/r. Equation (2.4) has the solution

$$y_n = A\cos\omega_n t + B\sin\omega_n t \tag{2.5}$$

$$\omega_n = \sqrt{\frac{k}{m}(\beta_n^2 + 1)} \tag{2.6}$$

At time $t = 0$, $\dot{y}_n = v_0$ and $y_n = 0$. Substituting these conditions into Equation (2.5) results in the following equations for the vertical displacement, velocity, and acceleration of the nose:

$$y_n = \frac{v_0}{\omega_n} \sin \omega_n t \tag{2.7}$$

$$\dot{y}_n = v_0 \cos \omega_n t \tag{2.8}$$

$$\ddot{y}_n = -v_0 \omega_n \sin \omega_n t \tag{2.9}$$

The angular quantities are determined by substituting Equation (2.9) into Equation (2.3) and integrating.

$$\alpha = \frac{\beta_n v_0 \omega_n}{r(\beta_n^2 + 1)} \sin \omega_n t \tag{2.10}$$

$$\omega = \frac{-\beta_n v_0}{r(\beta_n^2 + 1)} [\cos \omega_n t - 1] \tag{2.11}$$

$$\theta = \frac{-\beta_n v_0}{r(\beta_n^2 + 1)} \left[\frac{\sin \omega_n t}{\omega_n} - t \right] + \theta_0 \tag{2.12}$$

These results are only valid during the time interval ($0 \leq t \leq \pi/\omega_n$) when the spring is in contact with the rigid surface. For times $t > \pi/\omega_n$ and before the tail contacts the rigid surface,

$$\alpha = 0, \tag{2.13}$$

$$\omega = \frac{2\beta_n v_0}{r(\beta_n^2 + 1)}, \tag{2.14}$$

$$\theta = \frac{\beta_n v_0}{r(\beta_n^2 + 1)} \left[\frac{-\pi}{\omega_n} + 2t \right] + \theta_0 \tag{2.15}$$

2.2.3 Velocity of Tail at Impact

The vertical velocity at the tail of the body v_t is related to the vertical velocity and angular velocity at the nose by

$$v_t = v_n + \omega(l_n + l_t) \cos \theta \tag{2.16}$$

where $v_n = \dot{y}_n$. Substituting Equations (2.8) and (2.11) into the above equation and assuming that $\cos \theta \approx 1$, the ratio of the velocity at the tail to the initial vertical velocity is:

$$\frac{v_t}{v_0} = \cos \omega_n t - \frac{\beta_n(\beta_n + \beta_t)}{(1 + \beta_n^2)} [\cos \omega_n t - 1] \tag{2.17}$$

where β_t is defined to be l_t/r. This ratio is maximized at time $t = \pi/\omega_n$ and gives a maximum velocity ratio of

$$\frac{v_t}{v_0} = \frac{2\beta_n(\beta_n + \beta_t)}{1 + \beta_n^2} - 1 \tag{2.18}$$

This result indicates that if linear elastic response is assumed, the magnitude of the slapdown velocity of the body can be estimated using only geometric and mass quantities; the force-displacement behavior of the body is not needed. Furthermore, Equation (2.18) can be used to show that

$$\text{If} \quad \beta_n \beta_t \leq 1, \quad \text{then} \quad \frac{v_t}{v_0} \leq 1 \tag{2.19}$$

2.2.4 Effect of Inelastic Force-Displacement Behavior

The results in the previous section were derived assuming a linear elastic force-displacement behavior. In general, the force-displacement behavior is inelastic and energy is dissipated by plastic deformation. In this section it will be shown that when energy is dissipated by plastic deformation, the slapdown velocity ratio is closer to unity than if there is no energy dissipation.

In this derivation, the springs are assumed to have an infinite unloading modulus which means that all of the internal energy in the spring is dissipated. Equations (2.1) through (2.12) are still valid, except that the time interval is reduced to $(0 \leq t \leq \pi/2\omega_n)$. If the tail impacts the rigid surface at time $t = \pi/2\omega_n$, then Equation (2.17) gives the following expression for the maximum inelastic velocity ratio:

$$\frac{v_t}{v_0} = \frac{\beta_n(\beta_n + \beta_t)}{1 + \beta_n^2} \tag{2.20}$$

which can be written as:

$$\left(\frac{v_t}{v_0}\right)_\infty = \left(\frac{v_t}{v_0}\right)_E + \left(\frac{1 - \beta_n \beta_t}{1 + \beta_n^2}\right) \tag{2.21}$$

where the subscripts $(\ )_\infty$ and $(\ )_E$ denote infinite unloading modulus and elastic unloading modulus, respectively. The last term on the right-hand-side is greater than zero if $\beta_n \beta_t \leq 1$ and is less than zero if $\beta_n \beta_t \geq 1$. Therefore, an infinite unloading modulus results in a tip velocity ratio that is closer to unity than the velocity ratio calculated assuming linear elastic impact behavior. These two cases bound the possible unloading behavior of all bodies, therefore

$$\text{If} \quad \left\{ \begin{array}{lcl} \beta_n \beta_t & \leq & 1 \\ \\ \beta_n \beta_t & \geq & 1 \end{array} \right\}, \qquad \text{then} \quad \left\{ \begin{array}{lcl} \left[\frac{v_t}{v_0}\right]_E & \leq & \left[\frac{v_t}{v_0}\right]_I \leq 1 \\ \\ \left[\frac{v_t}{v_0}\right]_E & \geq & \left[\frac{v_t}{v_0}\right]_I \geq 1 \end{array} \right\}$$

where the subscripts $(\ )_E$ and $(\ )_I$ refer to the elastic and inelastic responses, respectively. The above results have been verified using the SLAPDOWN program. Note that although the velocity ratio for the inelastic case increases when $\beta_n \beta_t \leq 1$, it does not increase to greater than unity. If the body is symmetric, then $\beta_n = \beta_t$ and this result states that there will be no slapdown if $L/r < 2$.

2.3 Conclusions

An equation has been derived which gives a conservative estimate of the velocity ratio for slapdown of a body impacting a rigid surface. Only easily obtainable geometric and mass quantities are required. This equation can be used during the design process to help determine a body geometry which will minimize the slapdown potential.

Equation (2.15) can be used to determine the minimum initial drop angle θ_0 such that the secondary impact occurs at the same time or after the initial impact point has rebounded from the rigid surface. This angle is important for three-dimensional finite element analyses of the slapdown event. The drop angle is given by

$$\theta_0 = \frac{\beta_n v_0 \pi}{r(\beta_n^2 + 1)\omega_n} \tag{2.22}$$

This angle is measured counter-clockwise from the horizontal and assumes that the body has the same radius at the initial and secondary impact points. If the body is not symmetric, the angle $\tan^{-1}\left(\frac{R_n - R_t}{l_n + l_t}\right)$ must be subtracted from the initial angle θ_0 to account for the asymmetric geometry. R_n and R_t are the radii at the nose and tail of the body, respectively, and the radius is defined as the perpendicular distance from the longitudinal axis of the body to the impact point.

3. Description of SLAPDOWN Idealization

The idealization of the body and the numerical algorithms required to perform the spatial and temporal integration of the equations of motion in SLAPDOWN are described in this chapter. The idealized geometry is described in the first section; the next section describes the algorithms used to determine the spring and frictional forces at the impact points. The explicit time integration scheme is explained in the final section.

3.1 Geometry Idealization

The impact response of a deformable body is idealized in SLAPDOWN as a simple three degree-of-freedom body. The three degrees-of-freedom are the vertical, horizontal, and angular velocity at the center of gravity (CG) of the body. The nonlinear force-deformation response of the deformable body is represented by two piecewise linear "springs" which apply both a vertical force and a moment to the body. The springs are located at the initial and secondary impact points. A horizontal force and an additional moment are caused by frictional forces at the point(s) of impact. The mass of the body is assumed to be concentrated at the CG, and the idealization has the same mass moment of inertia as the body. Figure 3.1 shows a cross-section of the geometry being analyzed and the SLAPDOWN idealization.

End Treatment Two options are available for modeling the spring attachment to the body: SQUARE and ROUND. If the SQUARE option is used, the spring is constrained to be perpendicular to the axis of the rigid body; in the ROUND option, the spring is perpendicular to the rigid surface. Figure 3.2 illustrates these two configurations. In both cases, the force-displacement curve is defined in terms of the displacement normal to the rigid surface. The effect of the different end treatments is only important for large angle impacts; for shallow angle impacts the difference in the response is negligible.

3.2 Normal and Tangential Force Algorithms

The algorithms used to determine the normal and tangential forces resulting from the body deformation and friction between the body and the rigid surface are described in this section.

3.2.1 Normal Force—"Springs"

The normal force results from the deformation of the body after impact with the rigid surface. In SLAPDOWN, a piecewise linear spring definition is used to approximate

the force-deformation behavior of the actual body. An unloading modulus can also be specified which represents the force-displacement behavior during rebound of the body. In this way a plastic spring can be modeled. If the unloading modulus is not specified, the body unloads along the original loading curve simulating a non-linear elastic spring. The spring reloads along the same path as it unloaded.

The algorithm that implements this behavior requires three variables in addition to the spring definition: (1) the current spring displacement, DISP, (2) the maximum spring displacement, DISPMX, and (3) a logical variable to determine if the spring has rebounded. If the spring has not yet rebounded and is still loading, the algorithm simply searches the spring definition until the value of DISP is bounded by the displacement values of one of the piecewise linear spring segments. It then linearly interpolates to find the corresponding force. If the value of DISP is larger than the maximum displacement in the spring definition, an error message is printed and the program stops.

If the value of DISP is less than the value of DISPMX, the spring is unloading. Two options are used to determine the spring force. If the unloading modulus (UNLOAD) is zero, the unloading path is along the spring definition curve, and the force calculation proceeds as described in the previous paragraph. If the unloading modulus is nonzero, the algorithm must unload at that slope from the value of the maximum displacement. The force corresponding to the maximum displacement DISPMX is calculated using the method described in the previous paragraph. The force is then reduced by the product of the unloading modulus and the rebound from the maximum spring displacement. The spring force must be non-negative at all times; if the calculated force is tensile, then the spring force is set to zero.

3.2.2 Tangential Force—Friction

The tangential force is the result of friction at the point of impact of the body with the rigid surface. The tangential force is equal to the product of the coefficient of friction, CF, and the normal force, FRC. The direction of this force is opposite to the direction of the horizontal velocity at the impact point; no force is applied if the horizontal velocity is zero.

The current algorithm has problems with high coefficients of friction and when both ends are in contact with the rigid surface. Methods for more accurately representing the frictional force are being developed and will be implemented when they have been thoroughly tested.

3.3 Explicit Time Integration

SLAPDOWN uses a central difference scheme to integrate the equations of motion through time. Table 3.1 is a flowchart for the explicit algorithm [1]. In the table, $\mathbf{u}$, $\dot{\mathbf{u}}$, and $\ddot{\mathbf{u}}$ are the displacements, velocities, and accelerations of the three degrees-of-freedom,

respectively; $\mathbf{f}_{ext}$ are the external forces due to the deformation of the springs and friction at the impact point; $\mathbf{M}$ is the mass matrix; N is the step number; and Δt is the time increment. A constant time increment Δt is used in SLAPDOWN.

---

1. Set initial conditions: $\mathbf{u}^0 = \mathbf{u}(0)$, $\dot{\mathbf{u}}^{1/2} = \dot{\mathbf{u}}(0)$, $\mathbf{f}_{ext}^0 = \mathbf{0}$, $N = 0$
2. Update displacements: $\mathbf{u}^{N+1} = \mathbf{u}^N + \Delta t \dot{\mathbf{u}}^{N+1/2}$
3. Compute external forces $\mathbf{f}_{ext}^{N+1}$ due to "springs" and friction
4. Update accelerations: $\ddot{\mathbf{u}}^{N+1} = \mathbf{M}^{-1}\mathbf{f}_{ext}^{N+1}$
5. $N \leftarrow N + 1$
6. Update velocities: $\dot{\mathbf{u}}^{N+1/2} = \dot{\mathbf{u}}^{N-1/2} + \Delta t \ddot{\mathbf{u}}$
7. Go to step 2

Table 3.1. Flowchart for explicit integration of equations of motion

The central difference method is conditionally stable. The stable time step for this method is:

$$\Delta t \leq \min \left[\frac{2}{\omega_n} \left(\sqrt{1 + \xi_n^2} - \xi_n \right) \right] = \Delta t_{\text{stab}}$$

where ω_n is the natural frequency of the system and ξ_n is the fraction of critical damping in the n^{th} mode. No damping is used in SLAPDOWN so the stable time step calculation reduces to:

$$\Delta t_{\text{stab}} = \frac{2}{\omega_{\max}}$$

The value of Δt_{stab} is calculated internally in SLAPDOWN; it is then reduced by the TIME STEP SCALE FACTOR read from the input file. The default value of the TIME STEP SCALE FACTOR is 0.1 (see Table A.2, page 55). The reduction is not required for stability, rather it is done for added resolution and improved accuracy.

The following equation is used to determine the value of ω_n that is used to calculate the stable time step interval. Note that $\lambda = \omega^2$ and $|\cdot|$ represents the determinant. The horizontal degree-of-freedom is not used in the calculation.

$$\begin{vmatrix} k_n + k_t - M\lambda & k_n l_n - k_t l_t \\ k_n l_n - k_t l_t & k_n l_n^2 + k_t l_t^2 - I\lambda \end{vmatrix} = 0$$

where k is the maximum spring constant in the spring definition, l is the length from the CG to the impact point, M is the mass, I is the moment of inertia, and the subscripts $(\cdot)_n$ and $(\cdot)_t$ refer to the nose and tail of the body, respectively.

This equation is based on the assumption that both springs remain in contact with the rigid surface and provide a tensile force when stretched. In SLAPDOWN, the springs release from the rigid surface and provide no tensile forces. To accommodate this feature,

the above calculation is repeated three times with different values for k_n and k_t; the minimum value calculated for Δt_{stab} is used. The three calculations are: (1) both ends in contact, (2) nose in contact, tail released ($k_t = 0$), and (3) tail in contact, nose released ($k_n = 0$).

The integration is stepped through time using the calculated value of Δt until either both springs have unloaded, or the velocities of both the NOSE and TAIL are positive. Data are written to the EXODUS postprocessing file at both the first and last time step and every PLOT (see Table A.2, page 55) steps throughout the analysis.

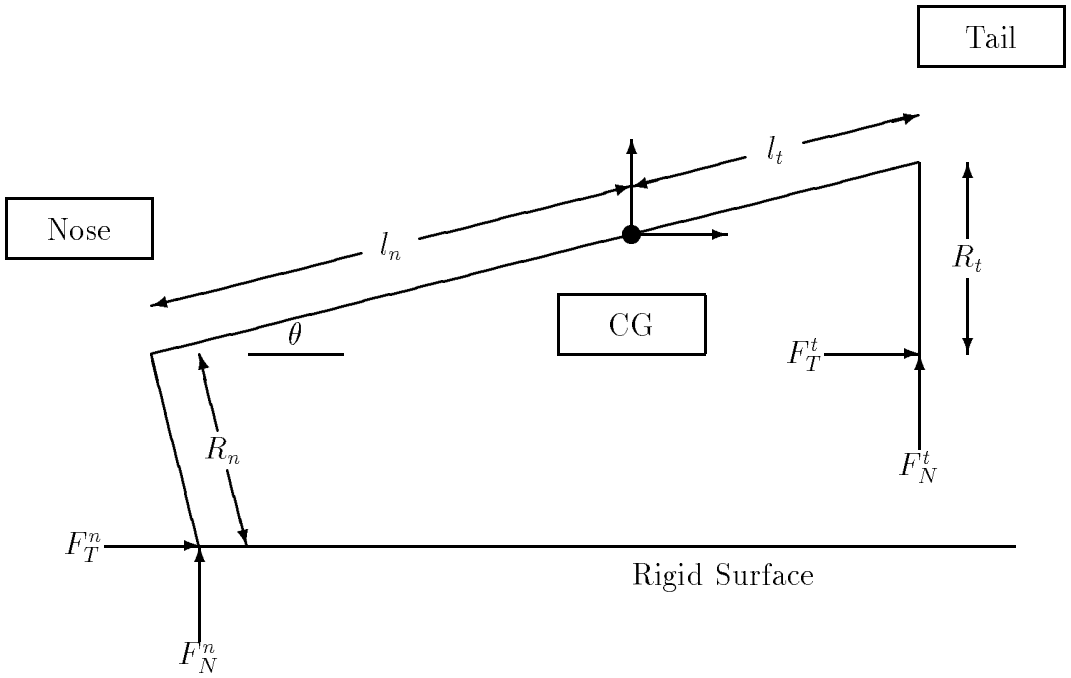

Figure 3.1. SLAPDOWN Geometry Idealization (SQUARE end)

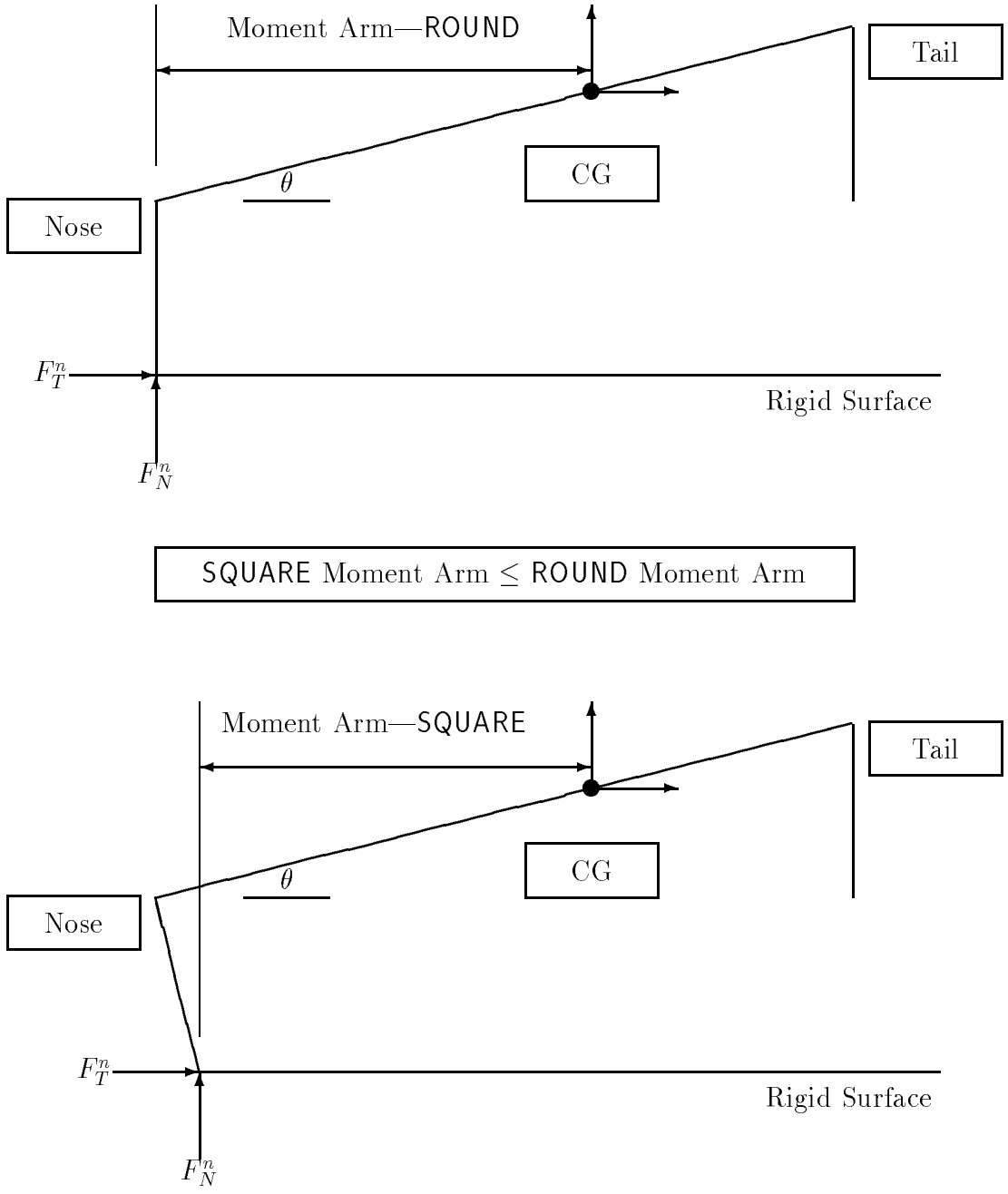

Figure 3.2. Effect of ROUND and SQUARE End Treatment

4. Effect of Aspect Ratio

4.1 Introduction

An important issue for radioactive materials transportation casks is the aspect ratio at which shallow angle slapdown impact events result in a higher velocity secondary impact than primary impact. Two primary parameters have been identified, slenderness and location of the center of gravity.

4.2 Slenderness

The slenderness issue was studied using solid and hollow cylinders (simple models which capture the essential geometry of most radioactive materials transportation casks). For the solid cylinder model, the initial geometry had a radius of 30 and a length of 120. The length was reduced in steps to 50 while the radius was increased to keep the overall model volume constant. The hollow cylinder model was treated similarly. The initial hollow cylinder model had a length of 120 with an outer radius of 30 and an inner radius of 21.21. These radii gave a cross-sectional area of the hollow cylinder equal to half the area enclosed by the outer radius. As for the solid cylinder, the length was reduced to 50 while the overall model volume and the relationship between cross-sectional areas were held constant. The details of the model geometries are shown in Tables 4.1 and 4.3. The slapdown analysis was performed for an initial angle of 15°. Two linear springs were investigated, one of which was elastic and the other plastic. The elastic spring had a linear spring constant for both loading and unloading of 600,000. Thus no energy was absorbed in the spring. The plastic spring had a loading constant of 600,000 (same as the elastic spring) but had an unloading constant of 600,000,000,000 (6 orders of magnitude higher than the loading constant). The effect of this high unloading constant was to prevent energy being returned to the structure on spring unloading thus giving an almost perfectly plastic spring. The initial angle of 15° was sufficient to ensure that for all cases, the nose was rebounding from the target prior to the tail impact. No frictional effects were considered here.

The results of the slapdown analysis for the solid cylinders with elastic and plastic springs are presented in Tables 4.1 and 4.2 respectively. For the hollow cylinders, the results are shown in Tables 4.3 and 4.4. The ratio of length to radius of gyration (L/r) was selected to describe the slenderness of an object subjected to shallow angle slapdown. The vertical velocity of the tail at the secondary impact and the maximum tail spring displacement were chosen to represent the severity of the secondary impact event. The maximum spring displacement is directly related to the energy required to stop the tail

Table 4.1. Effect of Aspect Ratio on Slapdown for Solid Cylinder Model with a Linear-Elastic Spring

Length	Outer Radius	Moment of Inertia	Radius of Gyration	Aspect (L/r)	Tail Velocity	Tail Displ
120	30.00	114,000	37.75	3.18	−979	6.028
80	36.75	69,700	29.51	2.71	−831	5.689
60	42.33	60,000	27.39	2.19	−613	4.745
55	44.31	59,400	27.25	2.02	−526	4.243
50	46.48	61,200	27.26	1.83	−409	3.468

Analysis performed at the following initial conditions:

Initial vertical velocity	=	−527.5
Initial angle	=	15.0°
Total mass	=	80.0
Spring - elastic Load	=	600.0×10^3
Spring - elastic Unload	=	600.0×10^3

Table 4.2. Effect of Aspect Ratio on Slapdown for Solid Cylinder Model with a Plastic (Energy-Absorbing) Spring

Length	Outer Radius	Moment of Inertia	Radius of Gyration	Aspect (L/r)	Tail Velocity	Tail Displ
120	30.00	114,000	37.75	3.18	−754	5.031
80	36.75	69,700	29.51	2.71	−678	4.804
60	42.33	60,000	27.39	2.19	−567	4.426
55	44.31	59,400	27.25	2.02	−523	4.261
50	46.48	61,200	27.26	1.83	−465	3.990

Analysis performed at the following initial conditions:

Initial vertical velocity	=	−527.5
Initial angle	=	15.0°
Total mass	=	80.0
Spring - plastic Load	=	600.0×10^3
Spring - plastic Unload	=	600.0×10^9

Figure 4.1. Effect of Aspect Ratio (L/r) on Slapdown Severity

of the object while the vertical velocity at impact provides a clear representation of the slapdown event independent of the tail spring characteristics. Tail vertical velocity at impact, non-dimensionalized by the initial velocity, is plotted against aspect ratio for both the solid and hollow cylinders in Figure 4.1. In Figure 4.1, non-dimensional tail velocities less than one, indicate that slapdown did not occur (secondary impact was less severe than primary impact). Slapdown did not occur when the aspect ratio was less than 2 for both model geometries and both spring types. The plastic spring brings the tail velocity at secondary impact closer to the initial velocity for all aspect ratios. Thus, with the plastic spring, secondary impact velocities are lower for aspect ratios greater than 2 and higher (but still less than the initial velocity) for aspect ratios less than 2.

A secondary impact less severe than the primary impact has been shown, in Chapter 2, to be a general relationship for aspect ratios less than two. In Chapter 2, the aspect ratio was defined in terms of $\beta_n = l_n/r$ and $\beta_t = l_t/r$ where:

r is the radius of gyration,
l_n is the distance from the center of mass to the nose, and
l_t is the distance from the center of mass to the tail.

Here $l_n = l_t = \frac{L}{2}$, so that

$$\beta_n = \beta_t = \frac{L}{2r}. \tag{4.1}$$

Table 4.3. Effect of Aspect Ratio on Slapdown for Hollow Cylinder Model with a Linear-Elastic Spring

Length	Outer Radius	Inner Radius	Moment of Inertia	Radius of Gyration	Aspect (L/r)	Tail Velocity	Tail Displ
120	30.00	21.21	123,000	39.21	3.06	−944	5.974
80	36.75	25.99	83,200	32.25	2.48	−741	5.360
62	41.74	29.52	77,900	31.20	1.99	−508	4.128
55	44.31	31.34	79,100	31.44	1.75	−373	3.202
50	46.48	32.87	81,500	31.91	1.57	−261	2.315

Analysis performed at the following initial conditions:

Initial vertical velocity	=	−527.5
Initial angle	=	15.0°
Total mass	=	80.0
Spring - elastic Load	=	600.0×10^3
Spring - elastic Unload	=	600.0×10^3

Table 4.4. Effect of Aspect Ratio on Slapdown for Hollow Cylinder Model with a Plastic (Energy-Absorbing) Spring

Length	Outer Radius	Inner Radius	Moment of Inertia	Radius of Gyration	Aspect (L/r)	Tail Velocity	Tail Displ
120	30.00	21.21	123,000	39.21	3.06	−736	4.962
80	36.75	25.99	83,200	32.25	2.48	−633	4.659
62	41.74	29.52	77,900	31.20	1.99	−515	4.224
55	44.31	31.34	79,100	31.44	1.75	−448	3.896
50	46.48	32.87	81,500	31.91	1.57	−391	3.562

Analysis performed at the following initial conditions:

Initial vertical velocity	=	−527.5
Initial angle	=	15.0°
Total mass	=	80.0
Spring - plastic Load	=	600.0×10^3
Spring - plastic Unload	=	600.0×10^9

Thus

$$\beta_n \cdot \beta_t = \frac{L^2}{4r^2}. \tag{4.2}$$

As shown in Equation 2.3.19, the tail impact velocity is less than the nose impact velocity when

$$\beta_n \cdot \beta_t \leq 1 \tag{4.3}$$

or when

$$\frac{L}{r} \leq 2. \tag{4.4}$$

4.3 Center of Gravity Location

In most transportation systems, due to the impact limiters, closure systems, gamma shielding, and contents, the center of gravity rarely coincides with the midpoint between loading springs. Thus, variation in the location of the center of gravity are of concern for transportation system design. Two of the solid cylinder models, those with length 120 and length 55, were chosen to investigate this phenomenon. These two models provide a wide variation in aspect ratio (3.18 and 2.02, respectively). The center of gravity was shifted independently of all other parameters including the moment of inertia. A physical interpretation of this shift is difficult to provide. It can be regarded as resulting from the appropriate distribution of a variable density material within the confines of the solid cylinder model geometry. Alternately, it can be regarded as a structure with the given mass and moment of inertia placed at varying locations along a rigid massless bar. The elastic and plastic springs described in Section 4.2 were also used here.

The results of shifting the center of gravity axially on the two solid cylinder models are shown in Figure 4.2 and in Tables 4.5 and 4.6. As can be seen in these tables, both the aspect ratio and the nose spring characteristics, influence the effects shifting the center of gravity. For the long cylinder, the tail velocity is maximized when the center of gravity is at the 30% location (closer to the nose than the tail) for both the linear and the nonlinear springs. For the short cylinder, maximum tail velocity occurs when the center of gravity coincides with the cylinder center (50% location). As expected, for an arbitrary center of gravity location, maximum energy absorption at the tail does not coincide with maximum tail velocity. The maximum tail energy occurs at a different center of gravity location for each case investigated. For the long cylinder with an elastic nose spring, maximum tail energy occurs at a center of gravity location of 60% (slightly toward the tail). With a plastic nose spring, maximum tail energy occurs at the 90% location. For the short cylinder, the maximum tail energy center of gravity location is 70% for an elastic nose spring and 80% for a plastic nose spring.

Figure 4.2. Effect of the Location of the center of gravity on Slapdown Severity

Table 4.5. Effect of Shift of center of gravity on Slapdown for Solid Cylinder Model Length=120 with Elastic and Plastic Spring

Elastic Spring			Plastic Spring		
C. G. Location % Length	Tail Velocity	Tail Displ	C. G. Location % Length	Tail Velocity	Tail Displ
10	−406	1.557	10	−470	1.791
20	−967	4.085	20	−743	3.165
30	−1132	5.357	30	−827	4.080
40	−1093	5.865	40	−809	4.654
50	−979	6.028	50	−754	5.031
60	−847	6.065	60	−689	5.263
70	−721	6.049	70	−626	5.466
80	−608	5.945	80	−570	5.607
90	−501	5.613	90	−520	5.722

Analysis performed at the following initial conditions:

Initial vertical velocity	=	−527.5	Initial vertical velocity	=	−527.5
Initial angle	=	15.0°	Initial angle	=	15.0°
Total mass	=	80.0	Total mass	=	80.0
Spring - elastic Load	=	600.0×10^3	Spring - plastic Load	=	600.0×10^3
Spring - elastic Unload	=	600.0×10^9	Spring - plastic Unload	=	600.0×10^9

Table 4.6. Effect of Shift of center of gravity on Slapdown for Solid Cylinder Model Length=55 with Elastic and Plastic Spring

Elastic Spring			Plastic Spring		
C. G. Location % Length	Tail Velocity	Tail Displ	C. G. Location % Length	Tail Velocity	Tail Displ
10	No Hit	0.	10	−198	1.110
20	−193	1.146	20	−358	2.185
30	−401	2.658	30	−460	3.075
40	−500	3.655	40	−510	3.755
50	−526	4.243	50	−523	4.261
60	−508	4.522	60	−516	4.636
70	−467	4.562	70	−496	4.902
80	−416	4.398	80	−471	5.044
90	−361	4.048	90	−444	5.031

Analysis performed at the following initial conditions:

Initial vertical velocity	=	−527.5	Initial vertical velocity	=	−527.5
Initial angle	=	15.0°	Initial angle	=	15.0°
Total mass	=	80.0	Total mass	=	80.0
Spring - elastic Load	=	600.0×10^3	Spring - plastic Load	=	600.0×10^3
Spring - elastic Unload	=	600.0×10^9	Spring - plastic Unload	=	600.0×10^9

4.4 Conclusions

The ratio of length to radius of gyration is the most appropriate parameter to describe the body geometry for shallow angle slapdown. The conclusion reached in Chapter 2 for linear behavior, that for a length to radius of gyration ratio less than two, no slapdown (increase in tail velocity at impact) can occur, has been numerically confirmed for nonlinear spring behavior as well. It is difficult to draw general conclusions concerning location of the center of gravity. For off-center location of the center of gravity, a simple relationship between tail velocity at impact and required energy absorption no longer exists. The maximum tail velocity occurs at a different center of gravity location than does the maximum tail spring energy absorption. Therefore, severity of the secondary (tail) impact is difficult to define. Thus, off-center location of the center of gravity can have an important effect on slapdown but each case must be investigated individually.

5. Effect of Initial Impact

5.1 Introduction

The behavior of the initial contact point is critical to the behavior of the subsequent slapdown event. In this section the effect of various of load-displacement curve shapes (nonlinear springs) and various amounts of energy absorption (low or high unloading modulus) are investigated. As in the previous section, the solid cylinder of length 120 and radius 30 is used. The analysis was performed for an initial vertical velocity of -527.5 and an initial angle of 15°. The 15° initial angle was chosen to ensure that the initial nose impact was completely over (forces on the nose were zero) prior to contact of the tail spring. Thus for the cases of elastic nose springs, the nose rebound was complete and all recoverable energy had been retransmitted to the cylinder. The model, at a total mass of 80, has a moment of inertia of 114,000, a radius of gyration of 37.75, and a slenderness ratio of 3.18. The secondary impact severity is represented by tail velocity at impact and by maximum tail displacement. As before, a linear tail spring is used so that tail displacement is a measure of the energy the tail is required to absorb.

5.2 Nose Spring Definition

Seven nose springs were analysed. Three of the springs were linear elastic with spring rates that varied from soft (150,000) to moderate (600,000) to almost rigid (600,000,000,000). Two linear plastic springs were also used. The loading spring rate match the soft and moderate linear elastic springs but the unloading rate was very stiff (600,000,000,000). This resulted in a spring in which the loads were proportional to the displacement for comparison to the elastic springs but in which all the energy was absorbed in the spring (there was no rebound). Finally, two nonlinear springs were analysed. These springs had an initial spring rate of 400,000 for a unit displacement. After the unit displacement, the spring force was held constant at 400,000 for all subsequent displacement. In one case the spring unloaded along the initial 400,000 spring rate recovering a small portion of the stored energy. In the other case the unloading spring rate was 600,000,000,000 resulting in no significant energy recovery and thus no rebound. The load-displacement curves for these seven springs are shown in Figures 5.1-5.3.

5.3 Conclusions

The results of the slapdown analysis for the solid cylinder with these seven nose spring characteristics are presented in Table 5.1. As can be seen in Table 5.1, energy

Figure 5.1. Load versus Displacement (Spring Rate) Curves for the Linear Elastic Springs

Figure 5.2. Load versus Displacement (Spring Rate) Curves for the Linear Plastic Springs

Figure 5.3. Load versus Displacement (Spring Rate) Curves for the Nonlinear Springs

absorption is the only characteristic of the nose spring which significantly affects the secondary impact severity. This confirms the result of Equation 2.3.18 on Page 16, where it was shown that, for linear elastic springs, the tail impact velocity is a function of geometry only, and not of nose spring rate.

This conclusion must be modified for application to actual transportation systems. First, most impact limiting systems used for transportation systems are relatively symmetric. Therefore, a softer nose spring implies a softer tail spring. Thus, while the tail velocity and tail energy absorption do not change, the tail accelerations will be lower

Table 5.1. Effect of Initial Impact Resilience on Secondary Impact

Nose Spring Type	Nose Spring Displ	Nose Spring Energy	Nose Spring Energy Absorbed	Tail Vel	Tail Displ
Soft L-E	6.628	3.295×10^6	0.	-982	6.035
Med L-E	3.318	3.303×10^6	0.	-979	6.029
Rigid	0.003326	3.319×10^6	0.	-972	6.018
Soft L-P	6.637	3.304×10^6	3.304×10^6	-753	5.073
Med L-P	3.326	3.319×10^6	3.319×10^6	-754	4.993
Nonlin-E	8.699	3.280×10^6	3.080×10^6	-808	4.972
Nonlin-P	8.707	3.283×10^6	3.283×10^6	-751	5.102

than for harder springs. The second effect of the use of softer nose springs results from the larger displacements required to stop the nose. These larger nose displacements in turn result in the requirement of a larger initial angle to ensure that the initial nose impact is complete prior to tail contact. Provided the initial nose impact is complete, the severity of the tail impact will decrease with increasing initial angle.

6. Effect of Friction on Slapdown Severity

6.1 Introduction

Friction between the initial impact point and the target can have a significant effect on the secondary impact severity in a shallow angle slapdown event. The coefficient of friction is a significant parameter influencing the importance of friction. However, the radius at which the friction force acts (distance between the contact point and the axial centerline of the object) also plays a significant role. These two parameters are investigated here.

The solid cylinder with length of 120 and radius to the edge of the spring of 40 was used. The mass was 80, the moment of inertia was 114,000, the initial vertical velocity was -527.5 and the initial angle was 15°. The moderate stiffness linear elastic and the nonlinear plastic springs described in the section on nose spring effects (Chapter 5) were used.

Figure 6.1. Effect of Friction on Slapdown Severity

Figure 6.2. Effect of Spring Radius (Moment Arm) on the Modification of Slapdown Severity by Friction

6.2 Coefficient of Friction

The results of a study on the effect of coefficient of friction are shown in Table 6.1 and Figure 6.1. Friction had a much greater effect for the linear elastic spring than for the nonlinear plastic spring. Two parameters contributed to this difference. The normal forces, and thus the frictional forces, were much higher for the linear elastic spring. In addition, no energy was absorbed for the linear elastic spring compared to the large amount absorbed in the nonlinear plastic spring. Thus, energy dissipation due to friction had a proportionally greater effect on the linear elastic spring than on the nonlinear plastic spring. The increase in tail velocity for coefficient of friction of 0.4 over that of 0.3 for the linear elastic spring is due to the development of sufficient frictional force that the nose sticks (nose velocity in the x direction goes to zero). When nose sticking occurs, no further energy is dissipated by friction. Therefore, more energy remains to accelerate the tail resulting in higher tail velocities.

6.3 Radius of Spring

The effect of spring radius (distance between the contact point and the axial centerline of the object) is shown in Table 6.2 and Figure 6.2. The secondary impact severity decreases almost linearly with increasing spring radius for both linear and nonlinear springs. As in the coefficient of friction study (Section 6.2), and for the same reasons, the effect of spring radius was more pronounced for the linear elastic spring than for the

Table 6.1. Effect of Increasing Coefficient Friction on Secondary Impact

Linear Elastic Spring Coefficient of Friction	Tail Velocity	Tail Displacement
0.0	-979	6.028
0.1	-938	5.777
0.2	-891	5.490
0.3	-852	5.251
0.4	-865	5.331
Nonlinear Plastic Spring Coefficient of Friction	**Tail Velocity**	**Tail Displacement**
0.0	-752	5.103
0.1	-733	4.993
0.2	-711	4.894
0.3	-690	4.756
0.4	-686	4.760

nonlinear plastic spring. The spring radius is proportional to the moment arm over which the frictional forces act. Thus, increasing spring radius serves to retard rotation. Retardation of rotation decreases the secondary impact severity at the expense of increasing the initial impact severity (energy is shifted from secondary impact to primary impact).

6.4 Conclusions

It is difficult to make broad generalizations covering the effects of friction on the shallow angle slapdown problem. While friction always serves to decrease the severity of the secondary impact, in certain extreme cases, friction can increase the severity of the initial impact sufficiently that the initial impact is more severe than the secondary impact. In general, for geometries, impact limiter behavior, and coefficients of friction anticipated in transportation of radioactive materials, it will be conservative to neglect friction in the analysis of shallow angle slapdown events. However, if the impact limiter radius is large compared to the package length or the coefficient of friction is anticipated to exceed 0.3, neglecting friction can lead to significantly unconservative initial impact predictions.

Table 6.2. Effect of Increasing Spring Radius on Secondary Impact

Linear Elastic Spring Coefficient of Friction 0.2 Radius of Spring	Tail Velocity	Tail Displacement
40.	-891	5.490
50.	-871	5.365
60.	-849	5.232
80.	-802	4.942
100.	-748	4.614
120.	-689	4.250
240.	-455	2.828
360.	-261	1.661
Nonlinear Plastic Spring Coefficient of Friction 0.2 Radius of Spring	Tail Velocity	Tail Displacement
40.	-711	4.894
50.	-702	4.832
60.	-692	4.787
80.	-670	4.652
100.	-645	4.504
120.	-617	4.325
240.	-502	3.630
360.	-430	3.069

7. Scaling Behavior

7.1 Introduction

In the field of radioactive materials transportation cask design, testing of scale models is very important. In order to successfully utilize the results of scale model tests, the appropriate parameters and techniques for extrapolating the results to full-scale behavior must be identified. Because the accelerations of practical interest are sufficiently high, the effects of a one G (gravity) field are ignored in the following discussion.

7.2 Simplified Analysis for Linear Systems

For linear behavior, a simplified engineering approach to scaling relations can be applied. For radioactive materials transportation cask applications, the linear accelerations at various locations along the cask length tend to be the most important parameters. These accelerations are used primarily to assess inertial loads on bolted closures, cask contents and other components. Therefore, the discussion below centers on the scaling relations for acceleration values. A more complete description of scaling relations can be found in Table 7.1.

Linear acceleration of the center-of-gravity is described by the equation relating force (F), mass (M), and acceleration (a):

$$F = M \cdot a. \tag{7.1}$$

Angular acceleration about the center-of-gravity is similarly described by the equation relating torque (T), moment of inertia (I), and angular acceleration (α):

$$T = I \cdot \alpha. \tag{7.2}$$

For linear acceleration, the forces are proportional to the square of the linear dimensions of the body. The mass is proportional to the cube of the linear dimensions. Therefore, the acceleration of a full-scale object should be half that of a half-scale object.

For angular acceleration, the torques are proportional to the cube of the body scale (T = force $\cdot$ length, where force $\propto$ length^2). The moment of inertia is proportional to the fifth power of the body scale (I = mass $\cdot$ length^2, where mass $\propto$ length^3). Therefore, the angular acceleration of a full-scale object should be one fourth that of a half-scale

object. However, the linear acceleration of the end of an object is equal to the angular acceleration times a length dimension. Thus, the linear acceleration of the tip of a rotating full-scale object should again be half that of a half-scale object. Note, for simplicity of the argument and because we are primarily concerned with the tangential component of acceleration for shallow angle slapdown events, the inward component of acceleration (centripetal acceleration) due to the square of the angular velocity times the length has been neglected in this argument. Inclusion of centripetal acceleration does not change the stated conclusion.

7.3 Numerical Confirmation Using SLAPDOWN

Nonlinear behavior of the structure at the impact locations is much more common than linear behavior. Nonlinear behavior arises from both geometric and material properties sources. The nonlinear behavior is easily incorporated into numeric solution procedures such as those found in the slapdown analysis program, SLAPDOWN, discussed in this report. SLAPDOWN will therefore be used to address the effects of nonlinear behavior on the scaling relations for slapdown impact events. Two sets of analyses will be performed. First, an analysis of linear behavior will be compared to the results of the simple engineering analysis described above. Then, an analysis of nonlinear behavior will determine the effects of nonlinearity on the scaling relations derived for linear behavior.

7.3.1 Linear Springs

A simple solid cylinder was selected to demonstrate the scaling relations. No system of units was assumed, thus any consistent units may be applied. In full-scale, the cylinder was given a mass of 80, a length of 120 units, and a radius of 30 units resulting in a moment of inertia of 114,000. An identical spring at each end of the cylinder had a travel of 10 units with a spring rate of 600,000 and an identical unloading modulus (that is the spring was linear on both loading and unloading with no energy dissipation). This cylinder was impacted onto a rigid target at an initial angle of 10° with an initial velocity of 527.45. This velocity was selected, based on the author's bias, because it is consistent, in units of in/sec, with the NRC 30-foot free drop hypothetical accident condition. A solid cylinder consistent with the half- scale of the cylinder described above has a mass of 10, a length of 60 units, and a radius of 15 units for a moment of inertia of 3563. In half-scale, the spring travel was 5 units with a spring rate of 300,000 for both loading and unloading. The initial impact conditions were identical with those of the full-scale cylinder. The model description parameters are listed in Table 7.1 for easy comparison.

SLAPDOWN analysis results show that the sequence of events occurs at twice the speed for the half-scale cylinder as for the full-scale cylinder. The displacements for the half-scale cylinder are half the full-scale cylinder's displacements. Linear velocities are the same for both half- and full-scale cylinders, and linear accelerations of the half-scale cylinder are double those of the full-scale cylinder. The angular velocities of the half-scale

Table 7.1. Comparison of Full- and Half-Scale Linear Spring Models

	Full-Scale	Half-Scale	Ratio (Full/Half)
Geometry and Initial Conditions:			
Overall Length	120.0	60.0	2.0
Mass	80.0	10.0	8.0
Moment of Inertia	114000.0	3563.0	32.0
Spring Constants:			
Loading	600000.	300000.	2.0
Unloading	600000.	300000.	2.0
Initial Velocity	−527.5	−527.5	1.0
Initial Angle	10.0	10.0	1.0
Results:			
Maximum Accelerations			
Nose	85720.	171400.	0.5
	−67780.	−135600.	0.5
Tail	158400.	316700.	0.5
	−36610.	−73210.	0.5
C.-G.	45300.	90590.	0.5
	0.	0.	0.5
Angular	1893.	7583.	0.25
	−1023.	−4090.	0.25
Maximum Velocities			
Nose	536.4	536.4	1.0
	−527.5	−527.5	1.0
Tail	1.7	1.7	1.0
	−983.2	−983.2	1.0
C.-G.	56.7	56.7	1.0
	−527.5	−527.5	1.0
Angular	0.0	0.0	0.5
	−12.7	−25.3	0.5
Maximum Displacements			
Nose	3.28	1.64	2.0
Tail	6.04	3.02	2.0

Figure 7.1. Nose, Center-of-Gravity, and Tail Displacements versus Time for Full- and Half-Scale Cylinders with Linear Springs

cylinder are double those of the full-scale cylinder, and the angular accelerations for the half-scale cylinder are four times those for the full-scale cylinder. Thus, if an object has a non-zero angular velocity at impact, the half-scale object must have double the initial angular velocity of the full-scale object, for proper scaling. These results are shown in Figures 7.1-7.3. The maximum values of displacement, velocity, and acceleration are shown in Table 7.1.

7.3.2 Nonlinear Springs

To investigate the nonlinear behavior, the cylinders described above were again used. The only differences were the springs. For the full-scale cylinder, a spring with an initial spring rate of 750,000 for the initial travel of 2 units followed by a tangent spring rate of 0 for the next 8 units was selected. Thus the force curve rose linearly to a value of 1,500,000 and then remained at that value for the remainder of the compression. An unloading modulus of 600,000 was again selected. Since unloading occurs linearly from the maximum load reached, the spring selected has the potential to absorb a considerable amount of energy. The half-scale spring has an initial spring rate of 375,000 over the first unit of displacement. This force remains constant for the next 4 units of displacement. The unloading modulus is 300,000. The initial conditions for the impact event were identical with those described above for the linear analysis. The impact initial conditions and model description are shown in Table 7.2.

The results for the nonlinear springs showed exactly the same behavior as described

Figure 7.2. Nose, Center-of-Gravity, and Tail Velocities versus Time for Full- and Half-Scale Cylinders with Linear Springs

Figure 7.3. Nose, Center-of-Gravity, and Tail Accelerations versus Time for Full- and Half-Scale Cylinders with Linear Springs

Table 7.2. Comparison of Full- and Half-Scale Nonlinear Spring Models

	Full-Scale	Half-Scale	Ratio (Full/Half)
Geometry and Initial Conditions:			
Overall Length	120.0	60.0	2.0
Mass	80.0	10.0	8.0
Moment of Inertia	114000.0	3563.0	32.0
Spring Constants:			
Loading section 1	750000.	375000.	2.0
Loading section 2	0.	0.	2.0
Unloading	600000.	300000.	2.0
Initial Velocity	−527.5	−527.5	1.0
Initial Angle	10.0	10.0	1.0
Results:			
Maximum Accelerations			
Nose	65630.	131300.	0.5
	−28760.	−57530.	0.5
Tail	66260.	132500.	0.5
	−28130.	−56260.	0.5
C.-G.	18750.	37500.	0.5
	0.	0.	0.5
Angular	788.5	3154.	0.25
	−781.5	−3126.	0.25
Maximum Velocities			
Nose	409.5	409.5	1.0
	−527.5	−527.5	1.0
Tail	7.5	7.5	1.0
	−928.8	−928.8	1.0
C.-G.	6.6	6.6	1.0
	−527.5	−527.5	1.0
Angular	0.0158	0.0316	0.5
	−11.15	−22.3	0.5
Maximum Displacements			
Nose	3.16	1.58	2.0
Tail	7.53	3.77	2.0

Figure 7.4. Nose, Center-of-Gravity, and Tail Displacements versus Time for Full- and Half-Scale Cylinders with Nonlinear Springs

for the linear springs. Nonlinear behavior is shown in Figures 7.4-7.6 and the maximum values in Table 7.2.

7.4 Conclusions

In this section, we have shown that the results of impact testing scale models can easily be related to the behavior of full-scale objects. Model displacements can be related to full-scale object displacements by multiplying by the model scale. Model linear accelerations can be related to full-scale object linear accelerations by dividing by the model scale. Model angular accelerations can be related to those of the full-scale object by dividing by the square of the model scale. Linear velocities are identical between model and full-scale objects regardless of scale. Angular velocities scale in the manner of linear accelerations. The scaling relations for velocities indicate that the initial conditions for a model impact test should be identical to those expected for the full-scale event except for initial angular velocity. Initial angular velocity for the model should be inversely proportional to the scale of the model used. These scaling relations are summarized in Table 7.2.

Figure 7.5. Nose, Center-of-Gravity, and Tail Velocities versus Time for Full- and Half-Scale Cylinders with Nonlinear Springs

Figure 7.6. Nose, Center-of-Gravity, and Tail Accelerations versus Time for Full- and Half-Scale Cylinders with Nonlinear Springs

Table 7.3. Summary of Relationships for Scale Model Testing

Parameter	Scaling Relationships
Geometry and	
Initial Conditions:	
Overall Length	$l_{sm} = l_{fs} \times (Scale)^1$
Mass	$M_{sm} = M_{fs} \times (Scale)^3$
Moment of Inertia	$I_{sm} = I_{fs} \times (Scale)^5$
Spring Constants	$K_{sm} = K_{fs} \times (Scale)^1$
Initial Velocity	$V_{sm} = V_{fs} \times (Scale)^0$
Initial Angle	$\theta_{sm} = \theta_{fs} \times (Scale)^0$
Results:	
Linear Accelerations	$a_{sm} = a_{fs} \times (Scale)^{-1}$
Angular Accelerations	$\alpha_{sm} = \alpha_{fs} \times (Scale)^{-2}$
Linear Velocities	$V_{sm} = V_{fs} \times (Scale)^0$
Angular Velocities	$\omega_{sm} = \omega_{fs} \times (Scale)^{-1}$
Linear Displacements	$\Delta_{sm} = \Delta_{fs} \times (Scale)^1$
Angular Displacements	$\theta_{sm} = \theta_f \times (Scale)^0$

8. Conclusions

1. A simple three degree-of-freedom code, SLAPDOWN, has been written to approximate the eccentric impact response of a deformable body. Nonlinear load displacement characteristics and friction effects are included. The code has been verified experimentally and analytically. The code interfaces with Department 1520 plotting codes to provide convenient graphical output.

2. The secondary impact velocity of a body can be conveniently estimated using only the length and radius of gyration. Slapdown (velocity at secondary impact higher than the primary impact velocity) cannot occur for length to radius of gyration ratios less than two.

3. The amount of energy absorbed in the initial impact is the most important parameter associated with the nose spring characteristics. For linear elastic springs, the spring rate (stiffness) of the nose spring is unimportant.

4. Friction, for geometries and coefficients reasonably associated with transportation casks, has a small effect on secondary impact velocity. There is an optimum value (one which minimizes the secondary impact velocity) of coefficient of friction based on the load displacement characteristics of the nose spring and on the object geometry. Sufficient friction can increase the severity of the primary impact to values greater than those experienced for the flat side impact. This can make the primary impact at a shallow angle the controlling impact event.

5. The following scaling parameters have been verified for nonlinear as well as linear load displacement characteristics (one G field neglected):

Table 8.1. Summary of Relationships for Scale Model Testing

Parameter	Scaling Relationships
Geometry and	
Initial Conditions:	
Overall Length	$l_{sm} = l_{fs} \times (Scale)^1$
Mass	$M_{sm} = M_{fs} \times (Scale)^3$
Moment of Inertia	$I_{sm} = I_{fs} \times (Scale)^5$
Spring Constants	$K_{sm} = K_{fs} \times (Scale)^1$
Initial Velocity	$V_{sm} = V_{fs} \times (Scale)^0$
Initial Angle	$\theta_{sm} = \theta_{fs} \times (Scale)^0$
Results:	
Linear Accelerations	$a_{sm} = a_{fs} \times (Scale)^{-1}$
Angular Accelerations	$\alpha_{sm} = \alpha_{fs} \times (Scale)^{-2}$
Linear Velocities	$V_{sm} = V_{fs} \times (Scale)^0$
Angular Velocities	$\omega_{sm} = \omega_{fs} \times (Scale)^{-1}$
Linear Displacements	$\Delta_{sm} = \Delta_{fs} \times (Scale)^1$
Angular Displacements	$\theta_{sm} = \theta_f \times (Scale)^0$

References

[1] Belytschko, T., Overview of Semidiscretization, in: *Computational Methods for Transient Analysis*, T. Belytschko and T. J. R. Hughes, ed., Elsevier Science Publishers B. V., 1983.

[2] Mills-Curran, B., Gilkey, A. P., and Flanagan, D. P., "EXODUS: A finite element File Format for Pre- and Post-Processing," SAND87-2997, Sandia National Laboratories, Albuquerque, NM, 1988.

[3] Uncapher, W. L., Madsen, M. M., and Stenberg, D. R., "Side-Drop Development Testing in Support of the Defense High Level Waste Cask Program," SAND86-1332, Sandia National Laboratories, Albuquerque, NM, March 1988.

[4] Hallquist, J. O., "User's Manual for DYNA3D and DYNAP: Nonlinear Dynamic Analysis of Solids in Three Dimensions," UCID-19156, Lawrence Livermore National Laboratory, University of California, Livermore, California, July 1981.

[5] C. R. Adams, "GRAFAID Code User Manual Version 2.0," SAND84-1725, Sandia National Laboratories, Albuquerque, NM, September 1985.

Appendix A
SLAPDOWN User's Manual

SLAPDOWN is a computer program written to help analysts determine the behavior of a body impacting onto an unyielding surface. The program models the body as a three degree-of-freedom system. The deformation of the body is approximated by nonlinear springs at each end of the model. The program was written primarily to model the SLAPDOWN behavior of nuclear waste transportation casks subjected to the regulatory 30-foot drops onto an unyielding surface.

The theory and algorithms used within the program are described in Chapter 3. This Appendix describes the SLAPDOWN user interface and program execution.

A.1 Execution of the SLAPDOWN program

The SLAPDOWN executable and source files are located on the 1500 VAXCluster. The SLAPDOWN program is run by typing: SLAP *input_file* where *input_file* is the name of the file containing the input data. The file extension for this file must be `.INP`. To run SLAPDOWN interactively type: SLAP and input the required data from the terminal.

A.2 Description of SLAPDOWN Input Data

The input data to SLAPDOWN is a free field form using keywords. The keywords are intended to define a user friendly program language input. The input is order independent. The free field input allows the user to delimit entries by either a blank, a comma, or an equals sign. A dollar sign indicates that whatever follows on the line of input is a comment and is ignored. Although it is seldom necessary, an asterisk indicates that the current input line is to be continued on the next line.

The keyword input parsing is designed to allow the user to create readable input files. The parsing system used in SLAPDOWN examines only the first keyword and the last numerical constant found in the input line. For example, the two sample input lines below are both equivalent to the SLAPDOWN parser.

```
VERTICAL -527.5
VERTICAL VELOCITY IS -527.5 INCHES PER SECOND
```

Both of these lines set the initial vertical velocity to the value -527.5. Note that all of the words in the second line except for `VERTICAL` and `-527.5` are ignored by SLAPDOWN.

Table A.1. Keywords for SLAPDOWN—Geometric

Keyword	*Default*[1]	
HELP	—	
NOSE	—	Indicates that the geometric quantities following this line refer to the nose end of
TAIL	—	Indicates that the geometric quantities following this line refer to the tail end of
LENGTH	REQ	The length along the longitudin
RADIUS	REQ	The distance from the longitud
MU	0.0	
SPRING	REQ	Indicates the beginning of the spring definition, spring data
UNLOAD	0.0	

NOTE:
[1]'REQ' Indicates that a value must be input for this quantity; no default is supplied. '—' Indicates that this field is not applicable.

Tables A.1 and A.2 list the keywords recognized by SLAPDOWN. Normally, SLAPDOWN is run in a batch mode where the input data are read from the specified input file. In this mode the program prints an error message and then aborts if an incorrect keyword is entered. If SLAPDOWN is run interactively and an incorrect keyword is entered, the program prints a warning message and then returns to input mode so that the correct value may be entered. In both the interactive and batch mode, the program checks that all required values have been input. If it detects any undefined quantities, they are listed and the program terminates. A complete echo of the input data is written to the output file.

In the keyword list, the nose of the body refers to the part of the body in contact with the rigid surface at the beginning of the analysis. The tail of the body is the opposite end. The input quantities are divided into two types—geometric and global. Geometric quantities must be defined for both the nose and tail of the body. To select the correct end of the body in the input file type NOSE or TAIL, and then input the geometric quantities for that end. The global quantities are items, such as mass and moment of inertia, where only one value is required to describe the body. Global quantities may be input at any time. The first line of the input file must be a title which is used to identify the problem. The input phase is terminated by inputting either EXIT or END. A sample input file is shown in Figure A.1.

Table A.2. Keywords for SLAPDOWN—Global

Keyword	*Default*[1]	
HELP	—	Lists all keywords and th
MASS	REQ	
MOMENT	REQ	
VERTICAL	0.0	
HORIZONTAL	0.0	
THETA	0.0	Initial angle in degrees. Positive co
OMEGA	0.0	
GRAVITY	0.0	Constant vert
TIME	0.1	Time st
TERMINATION		Time to terminate the analysis. If TERMINATION is not specified, the
PLOT	1	The Plot data output interval specifies the number of time steps betwee
FRICTION	1.0	The friction factor is used to smooth the ap

NOTE:
[1]'REQ' Indicates that a value must be input for this quantity; no default is supplied. '—' Indicates that this field is not applicable.

A.3 SLAPDOWN Output Description

Two output files are created during the execution of the SLAPDOWN program: a text file containing an echo of the input data and a summary of the output data, and a binary plot file written in the EXODUS [2] format.

A.3.1 Text Output File

The text file written during execution of SLAPDOWN consists of four main sections. The first section describes the name of the program, the date of the latest program revision, the system hardware and software, and the time and date of execution.

The second section is a formatted echo of the input data. All input data appears in this section so that the input data file can be reconstructed at a later time.

The third section summarizes the sequence of events that occur during the analysis. The times at which the nose and the tail hit the impact surface and begin to rebound, the impact velocities, and the ratio of the impact and rebound velocities to the initial velocity are output.

The fourth section summarizes the results of the analysis. The minimum and maximum displacements, velocities, and accelerations of the nose, tail, and center of gravity are reported. These values provide an indication of the magnitude of the SLAPDOWN effect. Note that, unless a gravitational acceleration is specified, the acceleration of the center of gravity should always be greater than or equal to zero and therefore, the minimum velocity of the center of gravity should equal the initial velocity. Also, the maximum strain energy in each of the springs during the impact event is output. These values are important in determining the severity of the slapdown effect since for some geometries the second impact will occur at a velocity greater than the initial velocity; however, due to the bodies angular position and velocity, the strain energy in the spring will be less than that caused by a flat impact. The opposite effect will also occur (higher strain energy at lower impact velocity).

The name of this file is the same as the input data file except that the extension is `.OUT`. The file is named `SLAP.OUT` if the program is run interactively. Figures A.3 through A.6 illustrate the four sections of the output file resulting from the input shown in Figure A.1.

A.3.2 EXODUS Database File

A binary plot file is written to simplify postprocessing the results of the analysis. The file is written in the EXODUS database format. This database provides a link to the postprocessing codes used in Department 1520. Appendix ?? is a description of the EXODUS database format.

Table A.3. EXODUS Variable Names

Nodal variables:	
DISY	Vertical displacement
POSY	Vertical position
VELY	Vertical velocity
ACCY	Vertical acceleration
DISX	Horizontal displacement
POSX	Horizontal position
VELX	Horizontal velocity
ACCX	Horizontal acceleration
Element variables:	
FORCE	Normal force in the spring
FRICTION	Frictional force in the spring
Global variables:	
THETA	Angular position, Degrees
OMEGA	Angular velocity, Radians/time
ALPHA	Angular acceleration, Radians/time^2
KE	Kinetic energy
INTE	Internal strain energy in the spring
DAMKE	Damaging kinetic energy $= 1/2\left(mv_y^2 + I\omega^2\right)$

The output of SLAPDOWN consists of plot data for 8 nodal variables, 2 element variables and 6 global variables. The nodal variables are the positions, displacements, velocities, and accelerations in the horizontal and vertical directions of the nose, center of gravity, tail, and left and right spring contact points; the element variables are the normal and friction forces in the nose and tail springs; and the global variables are angular quantities (position, velocity and acceleration) and energies. The nose, center of gravity, and tail are designated as nodes 1, 2, and 3; the left and right spring contact points are designated as nodes 4 and 5; and the nose and tail springs are designated as elements 1 and 2, respectively. The variable names written to the EXODUS file are listed in Table A.3.

The name of this file is the same as the input data file with the suffix `.EXO`. The file is named `SLAP.EXO` if the program is run interactively.

```
CASK - TOP END HIT - LIN ELAS NOSE SPRING
NOSE, SQUARE
LENGTH 80
RADIUS 59.95
SPRING
  10.0 5.75E8
END

TAIL
LENGTH 88.35
RADIUS 49
SPRING
   0.1 2.28E7
  10.0 1.E8
END

MASS      839.8
MOMENT      3.287E+06
VERTICAL -527.5
THETA      10.00
TIME         .010
PLOT     1000
EXIT
```

Figure A.1. Sample input file for SLAPDOWN.

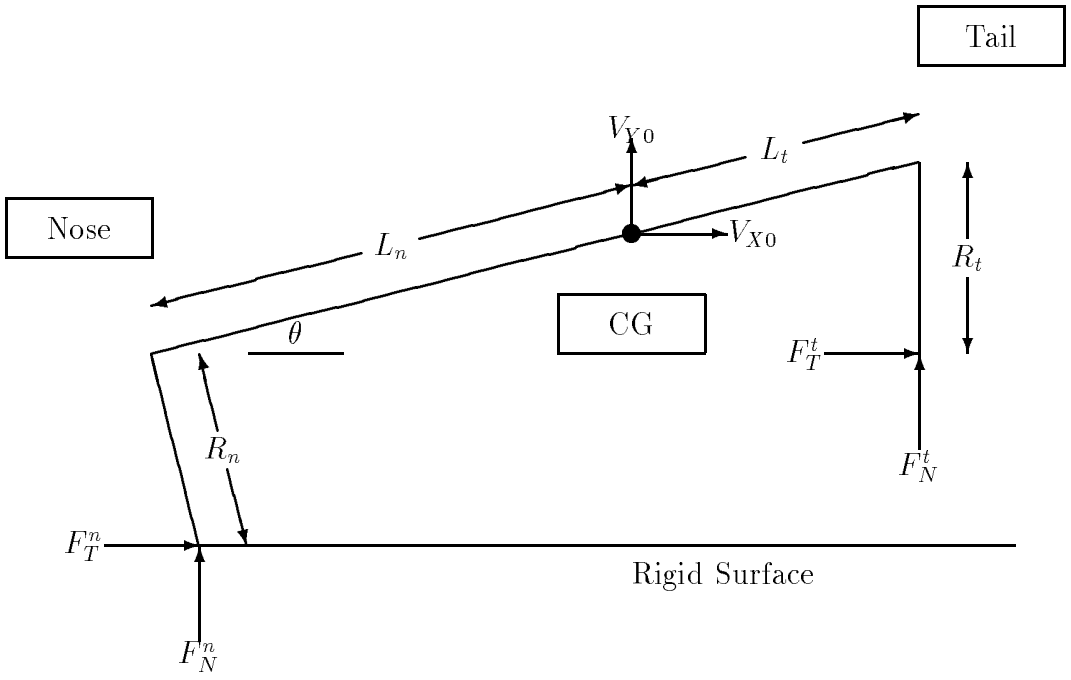

Figure A.2. SLAPDOWN Geometry Idealization (SQUARE end)

```
SLAPDOWN, Version 1.0
Run on 11/05/87 at 16:17:55
Compiled on a VAX 8600 using VMS 4.3.
```

Figure A.3. Sample output file for SLAPDOWN—Program Description

```
TITLE: CASK - TOP END HIT - LIN ELAS NOSE SPRING
****** NOSE PROPERTIES ******
LENGTH FROM NOSE TO CG (Z1)            8.000E+01
RADIUS OF CASK AT NOSE (R1)            5.995E+01
SQUARE END
COEFFICIENT OF FRICTION AT NOSE (CF1)  0.000E+00

       NOSE SPRING DEFINITION
       DISPLACEMENT     FORCE
         0.000E+00    0.000E+00
         1.000E+01    5.750E+08

UNLOAD ELASTICALLY ALONG SPRING CURVE

****** TAIL PROPERTIES ******
LENGTH FROM TAIL TO CG (Z2)            8.835E+01
RADIUS OF CASK AT TAIL (R2)            4.900E+01
COEFFICIENT OF FRICTION AT TAIL (CF2)  0.000E+00

       TAIL SPRING DEFINITION
       DISPLACEMENT     FORCE
         0.000E+00    0.000E+00
         1.000E-01    2.280E+07
         1.000E+01    1.000E+08

UNLOAD ELASTICALLY ALONG SPRING CURVE

****** MASS, MOMENT OF INERTIA, AND INITIAL CONDITION DATA ******
MASS OF BODY                           8.398E+02
MOMENT OF INERTIA                      3.287E+06
RADIUS OF GYRATION                     6.256E+01
INITIAL VERTICAL VELOCITY (pos. up)   -5.275E+02
INITIAL ANGLE (positive CCW)           1.000E+01
TIME STEP SCALE FACTOR                 1.000E-02
FRICTION SCALE FACTOR                  0.000E+00
WRITE PLOT DATA EVERY 1000 STEPS
TIP VELOCITY RATIO ESTIMATE            1.612E+00
```

Figure A.4. Sample output file for SLAPDOWN—Formatted Input Data Echo

```
****** S L A P D O W N ******

CASK - TOP END HIT - LIN ELAS NOSE SPRING

****** SEQUENCE OF EVENTS ******

** NOSE HIT     AT TIME  0.000E+00, VELOCITY = -5.275E+02
** NOSE REBOUND AT TIME  4.036E-03, VELOCITY =  4.421E+01
** NOSE UNLOAD  AT TIME  8.006E-03, VELOCITY =  6.133E+02
** TAIL HIT     AT TIME  5.108E-02, VELOCITY = -7.763E+02
** TAIL REBOUND AT TIME  5.742E-02, VELOCITY =  1.754E+00
```

Figure A.5. Sample output file for SLAPDOWN—Event Sequence

```
****** RESULTS ******

Event over at time    5.744E-02, Time step size  2.193E-05
Time step multiplier  1.000E-02,    4 Plot times written to database


           DISPLACEMENT     VELOCITY     ACCELERATION

   NOSE      1.358E+00      6.200E+02      2.226E+05 (MAX)
                           -5.275E+02     -3.553E+04 (MIN)

   TAIL      2.706E+00      4.983E+00      1.473E+05 (MAX)
                           -7.943E+02     -5.022E+04 (MIN)

     CG                    2.178E+02      9.299E+04 (MAX)
                           -5.275E+02      0.000E+00 (MIN)

ANGULAR                    0.000E+00      1.121E+03 (MAX)
                           -8.401E+00     -1.641E+03 (MIN)
```

Figure A.6. Sample output file for SLAPDOWN—Results Summary

Appendix B
Verification

B.1 Introduction

SLAPDOWN was verified by comparison of the analytical results of this code with accelerometer data from the half-scale Defense High Level Waste (DHLW) cask test program [3]. The half-scale DHLW cask geometry and instrumentation locations are shown in Figure B.1. The cask was dropped from a height of 30 ft. $\pm$ 1 in. at an initial angle of 10°$\pm$ 1°. such that the narrower end (opposite the closure) of the cask contacted the unyielding target first. Comparisons of experimental and analytical accelerations and velocities (integrated accelerations) were made at the accelerometer locations A7, A1, and A3. A7 is located on the cask bottom end (initial impact end). A1 is located slightly toward the closure from the center of gravity. A3 is located on the closure (secondary impact) end.

Figure B.1. Half-Scale DHLW Cask Model Instrumentation Drawing

Table B.1. Input Parameters to SLAPDOWN for the 30 Foot Drop Test of the DHLW Half-Scale Model at 10°

Geometry:	
Nose to CG	25.68
Tail to CG	23.5
Mass	15.2
Moment of Inertia	8900.
Nose Spring:	
Loading	400000. at 1.
	973000. at 3.
Unloading	8000000.
Tail Spring:	
Loading	388000. at 1.
	888000. at 2.8
Unloading	8000000.
Initial Conditions:	
Initial Velocity	−527.45
Initial Angle	10.

B.2 SLAPDOWN Input Development

A typical input to SLAPDOWN is shown in Table B.1. The total mass was determined from the measured weight of the half-scale cask. The moment of inertia was calculated from the geometry, weight, and location of the individual cask components. The moment of inertia calculation was not experimentally verified. The location of the cask center of gravity (length from nose to CG and tail to CG) was also calculated and verified experimentally. Agreement between the calculation and measurement of the center of gravity location was within .09 in.

The springs were defined using the results of finite element analysis and testing of a honeycomb structure similar to (but much simpler to analyse) that used for side impact limiters on the DHLW cask. A ring of aluminum honeycomb with an inside diameter of 20 in., an outside diameter of 31.75 in. and an axial length of 10.125 in. was applied to the axial center of a 5500 lb. cylinder. The honeycomb cell structure was aligned radially, as in the DHLW impact limiters. A sketch of the test structure is shown in Figure B.2. The cylinder was dropped from 15 and 22 ft. The cylinder drops were analysed using DYNA3D [4]. The analysis results for acceleration, final honeycomb crush (permanent impact limiter displacement), and footprint were in good agreement with the experimental results. These analysis results were then used to define the spring behavior of the DHLW impact limiters required by SLAPDOWN. The results for the 22-foot test cylinder drop were used because the amount of crush matched that expected in the DHLW

Figure B.2. Honeycomb Crush Test Structure

impact limiters due to a 30-foot drop. The acceleration of the center of gravity of the cylinder predicted by DYNA3D for the 22-foot drop is shown plotted against the center of gravity displacement in Figure B.3. This curve was smoothed, using the Butterworth low pass filter implemented in GRAFAID [5], to eliminate the contribution of the high frequency deformation modes to the acceleration. In order to apply a Butterworth filter, the curve must be single valued. A series of initial and trailing zeros will also facilitate the filtering operation. Thus the analytical curve of Figure B.3 was modified as shown in Figure B.4 by eliminating the unloading portion of the curve and adding the leading and trailing zeros. After filtering, the acceleration was converted into load by multiplying by the mass, and then scaled to the length used in the DHLW impact limiter. This result was approximated with bi-linear spring definition shown in Fig B.5 and used in the SLAPDOWN input described in Table B.1. The unloading modulus was estimated directly from Figure B.3. The effects of friction were ignored in the *spring* definition.

B.3 Comparison of SLAPDOWN with Experiment

The SLAPDOWN program writes results at the locations of the nose spring, the center of gravity, and the tail spring. For the half-scale DHLW cask test, these locations do not coincide with the accelerometer locations. However, because the cask is analysed as a rigid body, the analytical data may be determined at any arbitrary location by linear interpolation. Thus, the SLAPDOWN results were interpolated to be consistent with the accelerometer locations shown in Figure B.1.

Figure B.3. Acceleration versus Displacement for Honeycomb Crush Test Structure from DYNA3D for a 22-Foot Drop

Figure B.4. Acceleration versus Displacement for Honeycomb Crush Test Structure from DYNA3D for a 22-Foot Drop - Filtered

Figure B.5. Approximation of Load versus Displacement Behavior of Honeycomb Impact Limiters on the DHLW Half-Scale Model

Variation in drop height, within the experimental uncertainty, has a negligible effect on the cask behavior and thus was ignored. The initial angle, however, has an appreciable effect on the duration of the slapdown event along with a minor effect on the magnitudes of the accelerations and velocities. Therefore, slapdown analyses were run with initial angles between 9° and 14°. The values of acceleration and velocity from SLAPDOWN for the 13° initial angle are compared to the experimental data (at the three accelerometer locations A7, A1, and A3) in Figures B.6 - B.11. The 13° initial angle was chosen for display here because it provided the best match for the experimental data, perhaps indicating some rotation during the 30-foot free drop of the test.

Because the actual cask is not perfectly rigid, the accelerometers record some high frequency response. The experimental data in the Figures B.6 - B.11 has been filtered at 500 Hz to allow for easier comparison. 500 Hz was the lowest frequency which did not significantly alter the rise and fall times and the total pulse width of the data. Unfortunately, there is still a significant high frequency component in the accelerometer response remaining. Because of this remaining high frequency response, even after filtering, it is difficult to make accurate quantitative comparisons of acceleration values. However, when the accelerometer data are integrated to give velocities, the comparison is remarkably good. When the coarseness of the spring definition, the neglect of friction, and the experimental uncertainties are considered, these results indicate that slapdown events can be analysed with sufficient accuracy for a great number of purposes including determination of worst initial angles for testing and the effects of variations in impact

Figure B.6. Comparison of Analytical and Experimental Vertical Accelerations at Location A7

Figure B.7. Comparison of Analytical and Experimental Vertical Accelerations at Location A1

Figure B.8. Comparison of Analytical and Experimental Vertical Accelerations at Location A3

Figure B.9. Comparison of Analytical and Experimental Vertical Velocities at Location A7

Figure B.10. Comparison of Analytical and Experimental Vertical Velocities at Location A1

Figure B.11. Comparison of Analytical and Experimental Vertical Velocities at Location A3

limiter and cask parameters.